

# Design and Validation of a Push-Latch Gripper Made in Additive Manufacturing

Emilio Ottonello<sup>1,2</sup>, Mario Baggetta<sup>3</sup>, Giovanni Berselli<sup>1,3</sup>, and Alberto Parmiggiani<sup>1</sup>

## Abstract

The present paper describes the design, fabrication and validation of a push-latch gripper produced via Additive Manufacturing, which is capable of performing planar grasps of objects with two opposite parallel surfaces. In particular, the gripper modes of operation are presented, along with an efficient virtual prototype of the system based on a Pseudo-Rigid Body approximation. Such model is proven to be considerably more computationally efficient as compared to the corresponding Finite Element simulation, while still accurately capturing the fundamental behaviors of the mechanism. Finally, quantitative performance assessments are reported to practically show how Fused Filament Fabrication of Nylon components can be an excellent approach for creating monolithic robotic mechanisms with *embodied intelligence* that can be effectively employed for pick and place operations. Furthermore, this work represents one further example of an alternative approach to mechanisms development that combines part minimization, faster design iterations, and high repeatability.

## Index Terms

Compliant Mechanisms - Design Methods - Additive Manufacturing - Grasping & Manipulation - Industry Applications.

## I. INTRODUCTION

THE grasping operation is of crucial importance in the industrial automation sector, where it is commonly addressed using robotic grippers. In this field, the scientific literature is too vast to be comprehensively covered in the present paper. However, the review work by Zhang et al. [1] provides an exhaustive overview of the state of the art. The actuation system is possibly the best criterion for classifying different robotic grippers, which can be electric, pneumatic, hydraulic, vacuum, or magnetic. Among these, electric and pneumatic grippers are by far the most commonly used in automation settings [2]. In addition to the aforementioned established solutions, the literature on grippers presents many inventive and unconventional approaches, such as, e.g. [3].

In parallel, soft robotic grippers, i.e. those produced employing highly deformable materials with Young's modulus similar to biological tissues, are another class of devices with interesting characteristics. An early example of this approach is the pneumatic soft three-fingered gripper by Muscato et al. [4]. More recently, Deimel and Brock [5] introduced the *Pneuflex* design that has been released as open-source to support the replication of experiments. The traditional method for fabricating highly deformable parts relied on silicone molding, although recent developments in Additive Manufacturing (AM) enabled alternative fabrication approaches. For example, Drotman et al. [6] and Ge et al. [7] employed a Stratasys Connex multi-material 3D printer and a Digital Light Processing (DLP) printer to build soft pneumatic actuators. Other grippers, whose development heavily relied on AM, have been released as open-source models by the Yale OpenHand Project [8]. More in detail, several designs by Ma et al. [9] exploit the Hybrid Deposition Manufacturing (HDM) approach to fabricate soft multi-fingered, under-actuated robotic hands with rubber-like flexures having programmable stiffness. Furthermore, another class of unconventional soft grippers achieve their function by wrapping around the object to be grasped. Examples can be found in the works of Brown et al. [10], which introduced the concept of granular material jamming, Chen et al. [11], which presented an extensible origami gripper, and of Tsugami and Nishida [12], that created a soft magnetically actuated end-effector. Within the current vast literature on gripper design, also a variety of compliant and passive grippers have been proposed. Among compliant grippers, Wang et al. [13] employed a topology optimization approach to create a 2-degree-of-freedom (2DOF) compliant gripper. Meanwhile, McGowan et al. [14] developed a morphing compliant mechanism capable of separate gripping and retraction modes, utilizing a single actuation to achieve comparable grasp and retraction capabilities. Turning to passive grippers, Kodnongbua et al. [15] presented a computational design framework for the development of robotic end-effectors, specifically targeting passive solutions. In contrast, Hsiao et al. [16] proposed compliant bistable grippers that enable passive perching for UAVs (*Unmanned Aerial Vehicles*).

(Corresponding author: Emilio Ottonello.)

<sup>1</sup>Istituto Italiano di Tecnologia, Via San Quirico 19D, Genova - 16163, Italy (e-mail: emilio.ottonello@iit.it; alberto.parmiggiani@iit.it).

<sup>2</sup>Dipartimento di Informatica, Bioingegneria, Robotica e Ingegneria dei Sistemi [DIBRIS], Università degli Studi di Genova, Via Opera Pia 13, Genova, 16145, Italy

<sup>3</sup>Dipartimento di Ingegneria Meccanica [DIME], Università degli Studi di Genova, Via Opera Pia 15, Genova, 16145, Italy (e-mail: giovanni.berselli@unige.it; mario.baggetta@unige.it)

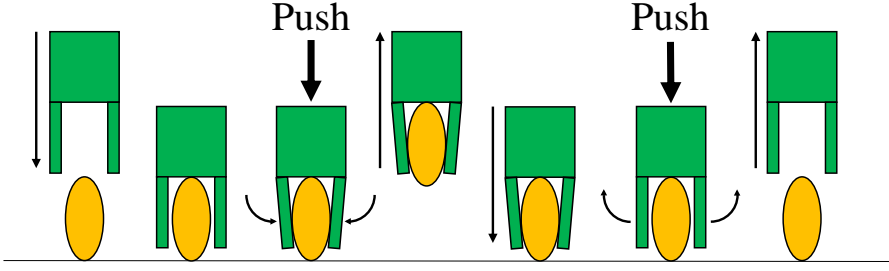


Fig. 1: Schematic operation of the proposed push-latch mechanism gripper.

#### *Contributions of the present work*

This paper describes the design, fabrication and validation of a “passive” monolithic gripper made in AM, whose operation relies on a push-latch mechanism hereafter named Push-Latch Gripper (PLG). Push-latch mechanisms are commonly employed in different engineering fields (e.g. SD (*Secure Digital*) insertion/ejection slots, furniture closures, etc.). While several implementations have been documented in the scientific and patent literature (see [17]–[19] for examples), to the best of the author’s knowledge, this work presents one of its first implementations in the design of robotic grippers.

The PLG mode of operation is shown Fig. 1: *i*) the gripper first approaches the object to be grasped; *ii*) when the object and the base of the gripper are in contact, further pushing causes the compliant fingers to close; *iii*) once the desired threshold is reached, the gripper fingers lock in place; *iv*) the grasped object can now be safely manipulated and moved; *v*) at last, an additional push is needed to release the part. Since the actuation of the gripper is obtained by moving it (e.g. with a robotic manipulator), the PLG is entirely passive and does not require additional power. This type of solution is not commonly employed in practice, possibly because of its low adaptability. However, industrial pick-and-place applications do not generally require a high degree of flexibility and adaptability, rendering grippers such as the PLG suitable for deployment in these contexts. Furthermore, the gripper presented in this work also exhibits the interesting features, namely:

- It is made via AM, thus allowing, fast development iterations and greater design freedom if compared to traditional processes [20]. Commercial grippers (e.g. the ones by Festo [21], Schunk [22], or BTM [23]) are generally made with metallic materials; in addition, the actuation of a commercial device often requires the integration of on-board complex systems or electronics or pneumatic lines. On the contrary, the PLG is manufactured with polymeric materials and does not require on-board drive systems. This aspect translates into a lower gripper weight.
- Conventionally designed devices are made of several parts assembled together; instead, the gripper presented in this work is monolithic [24], thus requiring no assembly operations. These mechanisms are peculiar because they can be immediately employed once manufactured which translates into time/cost savings. Since there is no need to precisely mate parts, fabrication processes with looser tolerances (therefore more affordable) can be adopted. Finally, as no components (e.g. fasteners, bearings, etc.) need to be integrated, monolithic systems often outperform their traditional counterparts in terms of weight.
- Another interesting feature of the current design is the adoption of compliant joints instead of rotational joints. In contrast to conventional kinematic pairs, compliant joints display a greater degree of predictability and durability owing to their immunity to wear, despite generally allowing lower ranges of motion. Compliant joints are also not affected by stick-slip friction thus tend to behave more predictably. This design approach lends itself well to AM implementations and several examples can be found in the literature [16], [25]–[27].

To summarize, the contributions of the paper are: *i*) introduction of a novel gripper design concept; *ii*) description of a computationally efficient method to virtually assess the PLG performance before physical prototyping; *iii*) experimental PLG validation.

## II. DESIGN OF THE SYSTEM

### A. System description

The PLG comprises two opposing fingers and, in the presented embodiment, it has been designed to grasp objects with two opposite parallel flat faces. When the gripper is pressed against the workpiece, the fingers approach the object and come into contact with its sides. This movement is obtained by employing the kinematic structure presented in the following sections. Figure 2 presents an illustration of the sequence of phases.

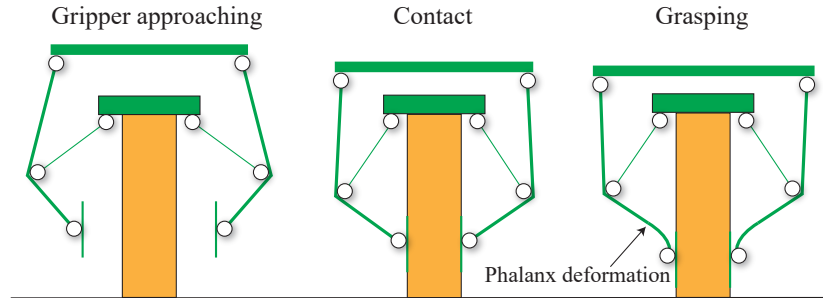


Fig. 2: Grasp sequence. The diagram represents the behavior of the gripper's mechanism in the three main phases of the grasping sequence.

The gripper can grasp objects in two main ways: by *force closure* (i.e. exploiting friction) or by *form closure*. These two grasping modalities are represented in Fig. 3.

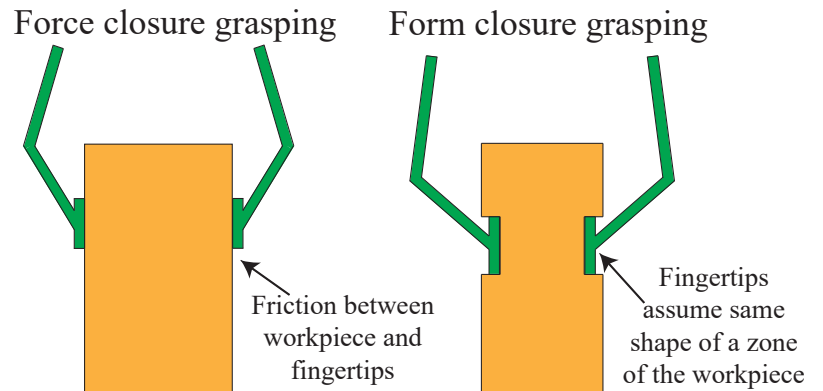


Fig. 3: Grasping modalities. The diagram represents the PLG force closure (left) and form closure (right) grasping modalities.

In force closure mode, the contact forces shall be sufficiently high to lift and move the object to be grasped. For such action to be possible, the friction force generated by the contact of the finger and the workpiece shall overcome the weight of the piece itself.

In the form closure operation mode, it is possible to implement fingers with custom shapes in their terminal part that geometrically adapt to the shape of the piece to be grasped. Naturally, the adoption of AM highly facilitates such approach. In both cases, when the gripper presses on the part, the motion of the platform, constrained by a linear guide, activates the fingers' movement. This movement, in turn, sets in motion a pin that slides inside a drive cam. Once the pin reaches a predefined position, the fingers are locked in the closed position. A further push results in the release of the push-latch mechanism and opening of the fingers. As previously mentioned, the PLG fingertip shape can be designed and manufactured to grasp objects with different geometries (not necessarily flat or planar), since the fingertip shape can be customized to match the specific morphology of the target object. On the other hand, due to its passive nature, the PLG architecture is not suitable for grasping families of objects with rather variable shape, although such drawback may be acceptable for application in industrial structured environments, where the PLG low-cost and ease-of-use are surely desirable. The PLG physical prototype is shown in Fig. 4, which also shows the indication and nomenclature of its main elements. To support the replication of the results of this work, the gripper's CAD (*Computer-Aided Design*) model has been publicly released on Github<sup>1</sup>. In addition, Fig. 5 depicts the PLG grasping sequence.

<sup>1</sup><https://github.com/made-iit/plg>

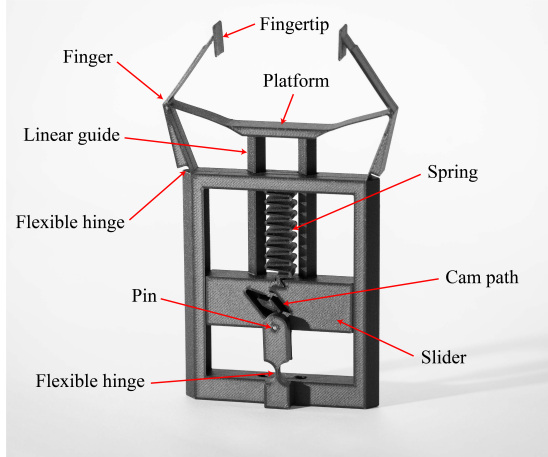


Fig. 4: PLG physical prototype (nomenclature included).

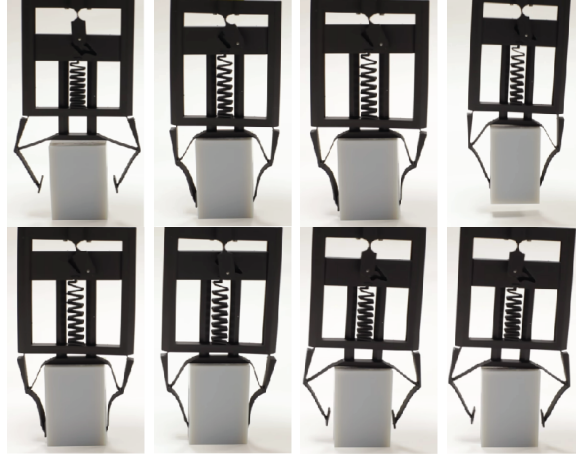


Fig. 5: Grasping sequence.

### B. Finger kinematics

The kinematics used for the design of the fingers is presented in Fig. 6. Given the system's symmetry, only half of the mechanism is depicted, including three moving bodies and the chassis (frame). The first body comprises the length strokes  $l_2$  and  $l_4$  rigidly connected at a fixed angle  $\gamma$ . The  $l_2$  section of the body lays at angle  $\theta_2$  with respect to the x-axis (i.e. the horizontal direction) in the rest position. A rod of length  $l_3$  connects the first body to the moving platform, i.e. the element pressing workpiece whose width is parametrized as  $w$ . The mechanism possess one DOF; as the moving platform translates downwards, the terminal part of the finger moves towards the symmetry axis.

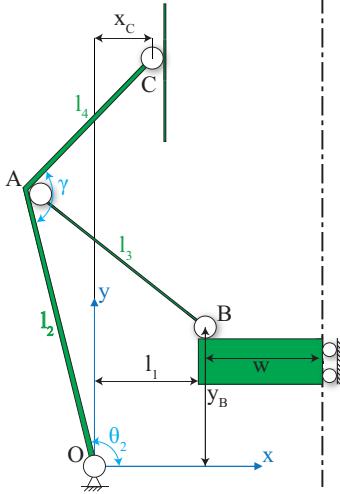


Fig. 6: Fingers kinematics. The figure presents the Rigid-Body topological model of the finger and the labels for the main geometric parameters and variables.

By imposing  $\theta_2$  as a free coordinate, the value of  $y_B$  is given in Eq. 1:

$$y_B = -l_2 \sin(\theta_2) + \sqrt{l_3^2 - (l_2 \cos(\theta_2) - l_1)^2} \quad (1)$$

The coordinate  $\theta_2$  is linked, in turn, to  $x_C$ , namely the horizontal coordinate of the contact plates. It will be necessary to have control over this amount to avoid collisions between the contact plates during the closing phase. The following equation holds:

$$\theta_2 = 2 \arctan\left(-\frac{-l_4 \sin(\gamma) + \sqrt{h^2 + l_4^2 \sin(\gamma)^2 - (k - x_C)^2}}{k - x_C - h}\right) \quad (2)$$

where  $k = w + l_1$  and  $h = l_2 - l_4 \cos(\gamma)$ . By imposing  $x_C$  with appropriate boundary conditions, one obtain constraints on  $\theta_2$  that, in turn, impose constraints on  $y_B$ . Ultimately, given the geometric size of the fingers, the overall platform displacement is found. As mentioned above, the employed joints are compliant. In particular, a *small-length flexural pivot* [28] has been used in point O, whereas the link  $l_3$  is realized as a deformable slender beam (i.e. it is realized with a lower thickness as compared to the other parts).

### C. Design for Additive Manufacturing

The PLG has been specifically designed to be fabricated via AM, and in particular, through *Fused Filament Fabrication* (FFF), also known as *Fused Deposition Modeling* (FDM) [29]. This particular technology consists of the deposition on a printing surface of softened material; the deposition takes place thanks to the movement of a moving head. Certain precautions must be taken to manufacture complex parts using this technology. The design of the PLG has been strongly influenced by the selected manufacturing technology. For example, the thickness of the compliant joints is limited by the printer's capabilities. Furthermore, the construction of the linear guides is performed so as to avoid using supports. The PLG has been manufactured with a *MarkTwo* printer by *Markforged* in *Onyx*, a *Nylon-12* reinforced with short carbon fibres. Onyx possesses good structural properties and the material's high value of deformation break (25%) makes it particularly suitable for constructing compliant mechanisms. The *MarkTwo* printer completed the PLG build in little less than six hours; the *Markforged* slicing software provided a cost estimation of 6.18€ (~ 6.65\$).

### D. Linear guides, positive drive cam, spring

With reference to Fig. 4, the vertical motion of the platform is obtained with a linear guide. In particular, the platform is integrated with an extension that slides relatively to the chassis. The extension is joined with the slider. The sliding of the guides is possible thanks to the special geometry of the parts. In particular, the joints must be stable, with a gap as narrow as possible and achievable without supports. Fig. 7 shows a representation of the cross-sectional views of the geometries used to construct linear guides. The gap width adopted in this work is 0.2[mm], namely the smallest value that allowed the free relative motion of the parts. The unsupported portions of the linear guides have been designed so as to lay at an angle of 45° to the build platform to enable support-free fabrication.

A positive drive cam mechanism, integrated into the slider, controls the fingers position. The cam follower consists of a metal pin installed on the gripper after the printing phase. As the pin advances through its path, it reaches four principal positions, represented in Fig. 8, whose function can be described as follows:

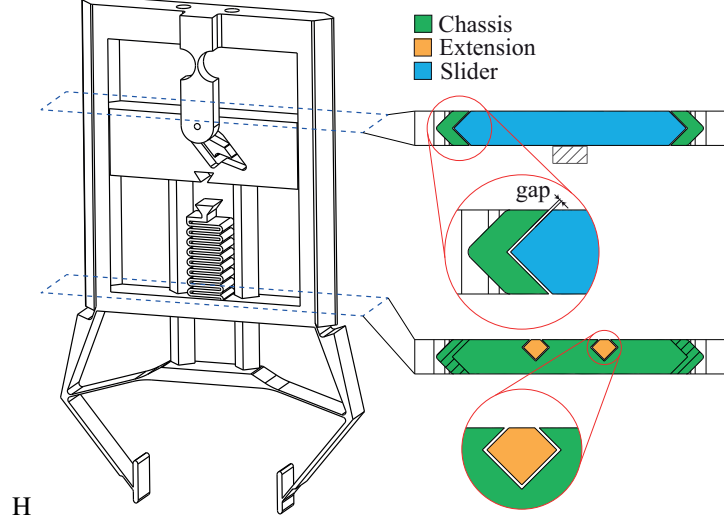


Fig. 7: Sections of linear guides.

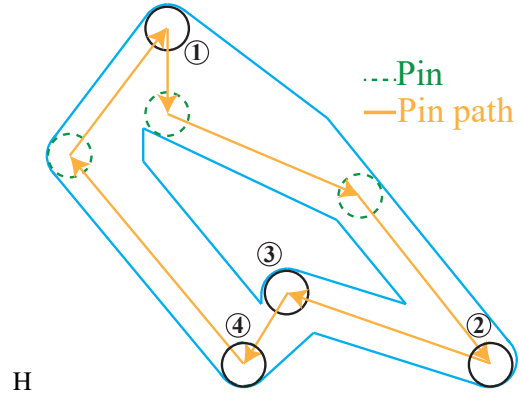


Fig. 8: Positive drive cam. The figure shows a cam path diagram and the phases of the motion of the guiding pin. The mechanism configurations from ① to ④ are explained in the text and used in subsequent figures.

- in the initial position, the fingers are open, and the pin is in the highest position (position ①);
- as the gripper pushes on the object to be grasped, the moving platform moves upward, thus moving the pin from the initial position to the lowest on the right (position ②);
- as the load is released, the pin moves to the position corresponding to the stable closing of the fingers (position ③);
- a further movement of the platform releases the pin, thus moving it to the low cam position on the left where the fingers are unlocked (position ④).

Finally, the elasticity in the mechanism brings the pin back to the initial position where the fingers are completely open. At last, a spring connecting the slider and the chassis assists the motion of the pin as it advances through the cam path. As depicted in Fig. 4, The spring is conceived employing a repeated S-shape; at the end of the printing phase, the spring has a shorter length than the distance to the slider. After printing, the spring is connected to the slider by extending it, thus applying a slight pre-load in the mechanism that aids its operation.

### III. PLG VIRTUAL PROTOTYPE

To validate the design of the gripper before physical testing, virtual simulations have been performed with the Finite Element Method (FEM) and also resorting to the Pseudo-Rigid Body (PRB) approximation solved using a commercial MultiBody Computer-Aided Engineering (CAE) tool, namely *Recurdyn*. Simulating the entire mechanism with the FEM approach requires a considerable computational effort, since a sufficiently dense mesh must be created and at least three contact pairs must be computed (i.e. two contact surfaces between fingertips and gripped part and a point contact between the pin of the cam mechanism and the corresponding guide). In order to simplify the virtual model and thus significantly reduce the computational time, a PRB counterpart of the FEM model has been derived, where the flexible parts of the mechanism are represented by rigid bodies connected by a series of spring-loaded joints. Once the kinematic pairs of the PRB model have been selected, an optimization routine is used to find the values for the position of the pivots and the stiffness of the springs that allow the

flexible kinetostatic behavior to be reproduced as accurately as possible. Details of the procedure are explained in [30]. A value of 1.4 [GPa] has been chosen for the material's elastic modulus to perform the simulations. This value is lower than the value provided in the manufacturer datasheet but agrees with experimental data from the literature [31], [32].

#### A. Spring and cam flexure PRB models

The pre-loaded spring can be easily approximated with a spring element in the *Recurdyn* software by using FEM simulations to measure the entity of the pre-load force  $F_{pre-load}$  and the stiffness coefficient  $K_{spring} = (F_{max} - F_{pre-load})/dx$ , as shown in Fig. 9. The same figure also shows the PRB equivalent model of the positive drive cam flexure. In this case, the value of the equivalent stiffness coefficient  $K_{cam}$  has been determined employing the *Recurdyn* built-in optimizer (as explained in [33]) so as to align the behavior of the PRB model to the corresponding FEM model. This procedure has been performed by applying a torsional moment  $M$  to the moving portion of the flexure while tracking the  $x$  and  $y$  displacements of the pin axis during the rotation; the optimization process for the stiffness value  $K_{cam}$  aimed at replicating the cam-end trajectory during deformation with the lowest possible error. The optimization routine have required a total of 52 simulations for a whole computational time of 18[s] on a workstation with an Intel(R) Xeon(R) CPU E3-1270 v5 @ 3.6 GHz and 32 GB RAM, obtaining a maximum trajectory error of less than 1%. Fig. 10 reports the spatial displacements of the FEM and optimal PRB model, showing the good accuracy achieved thanks to the optimization process.

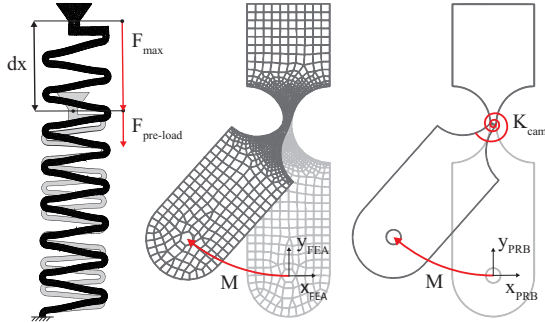


Fig. 9: 3D model view and PRB model of the compliant spring (left) and positive drive cam (right).

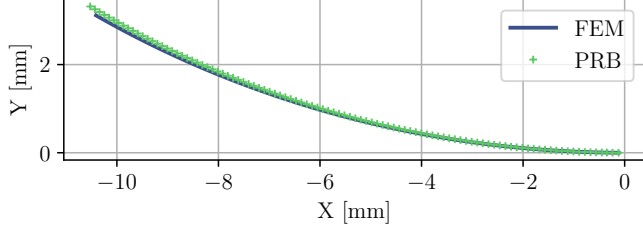


Fig. 10: Comparison between the flexible positive cam and equivalent PRB model: displacement plot.

#### B. Fingers PRM model

Unlike the positive drive cam, whose PRB approximation is proven to be acceptable employing a single torsion spring, the fingers of the proposed device require more parameters to be optimized, namely more torsion springs correctly placed are required in order to achieve an acceptable PRB approximation. In particular, after multiple trials, it has been chosen to approximate the two small length flexural pivots and the thickest beam ( $l_4$  as in Fig. 6) with single torsion springs, whereas the slender beam ( $l_3$ ) has been modeled employing four torsion springs, since this flexible segments is affected by the largest deformation (as suggested in [34]). Differently from the previous case and considering the nature and purpose of this component, the objective has been, in this case, to replicate in the PRB model the contact force  $F_c$  generated between the flexible finger and an object with a square cross-section of 21[mm] x 21[mm] during the first grasping phase of the gripper (i.e. from point ① to point ②, with reference to Fig. 8). As shown in Fig. 11, the variables to be optimized are the values of the four stiffness constants of the respective rotational springs and the value of the distance  $L$  between each extreme pair of springs attached to the smaller beam. This last optimization required a total of 153 simulations with a total computation time of 1120[s]; it is important to mention that the PRB model ran in about 7[s] instead of the 12600[s] required for the finite element model, with a maximum force error of less than 3.5%, which shows how useful this model is in terms of future optimization of the mechanism.

TABLE I: PRB model optimal parameters.

Subsystem	Variable	Value
Spring	$K_{spring}$	1.936 [N/mm]
	$F_{preload}$	4.22 [N]
Cam flexure	$K_{cam}$	120.745 [Nmm/rad]
Finger	$L$	1.403 [mm]
	$K_1$	196.043 [Nmm/rad]
	$K_2$	163.869 [Nmm/rad]
	$K_3$	65.933 [Nmm/rad]
	$K_4$	70.623 [Nmm/rad]

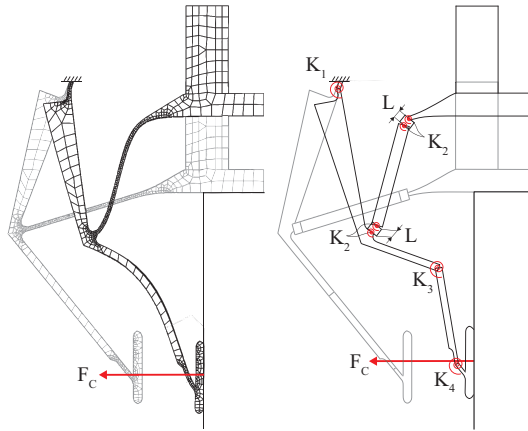


Fig. 11: 3D model view and PRB model of the gripper finger.

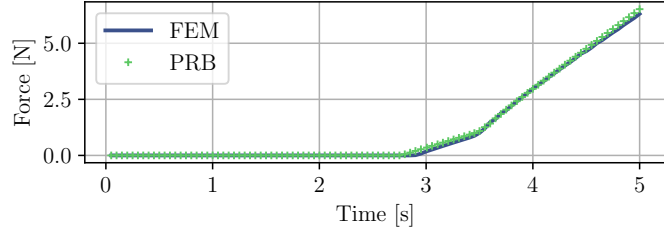


Fig. 12: Comparison between the flexible finger and equivalent PRB model: contact force plot.

Fig. 12 shows the comparison between the contact force values of the FEM and PRB models, whereas the optimal pivot positions and stiffnesses determined by the optimization routine are summarized in Table I.

### C. Gripper PRB model

After the optimization of the individual components of the gripper, the final step has been to perform a final simulation of the entire mechanism (see Fig. 13). By using the PRB model, the simulation of the whole gripping/releasing process of the component could be performed in significantly less time than what required for the flexible counterpart for the initial gripping process only (i.e., about 180[s] versus more than 27000[s]). The simulation is designed to reproduce the real behavior of the gripper and the same conditions as in the subsequent experimental tests (reported in detail in the next section). Thus, not only the contacts between the fingertips and the gripped component (orange in Fig. 13), but also the contact between the gripped component and the linear guide have been considered. This simulation made it possible to confirm the correct operation of the positive drive cam and to estimate, as a first approximation, the forces acting on the gripper. Fig. 14 shows the forces required to activate the mechanism with and without the part to be gripped (i.e. 83[N] and 44[N], respectively), whereas Fig. 15 shows the measured gripping force of the device, which is about 5[N] when the positive drive cam is in the lowest stable configuration (i.e. position ③).

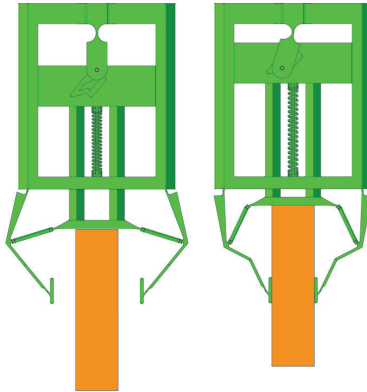


Fig. 13: PRB model of the gripper.

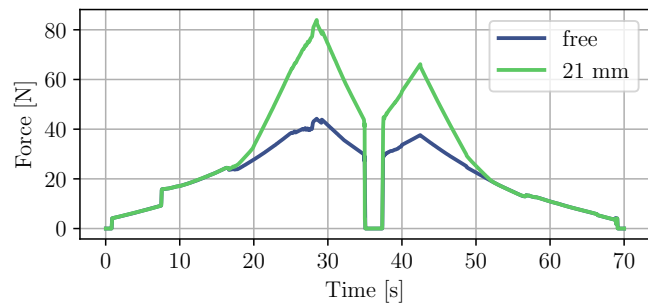


Fig. 14: PRB model: loading simulation with and without workpiece.

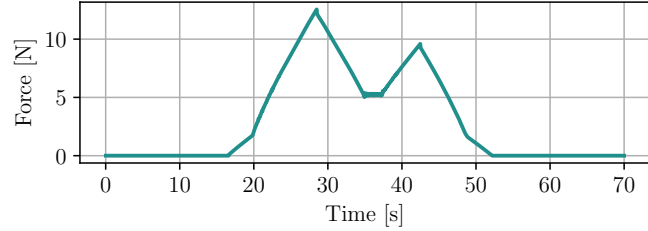


Fig. 15: PRB model: gripping force with a 21[mm]x21[mm] square cross-section object.

#### IV. MECHANICAL CHARACTERIZATION

##### A. Test campaign

As mentioned in the introductory section, the gripper presented in this work has been designed for handling objects with two opposite parallel flat faces. The following tests have been conducted to evaluate the gripper's performance quantitatively.

- 1) **Locking/unlocking test without workpiece.** The gripper is operated without a workpiece while measuring the force and displacement needed to close and open the fingers; this test quantifies the forces needed to operate the push-latch mechanism.
- 2) **Locking/unlocking test with workpieces.** The gripper is operated with workpieces of varying dimensions while measuring the force and displacement needed to close and open the fingers; this test quantifies the additional forces needed for grasping the workpieces.
- 3) **Force closure pull-out test.** The force necessary to remove the object from the gripper when the friction force operates is measured with varying workpiece dimensions. This test allows quantifying the maximum load bearable by the gripper by friction force given the size of the grasped object.
- 4) **Form closure pull-out test.** The force necessary to remove the object from the gripper when the coupling of shape operates is measured. This test allows quantifying the maximum load bearable by the gripper when shape coupling is employed.

The locking/unlocking tests (with and without workpieces) have been conducted with a *Zwick Roell Z050* testing machine. The machine is equipped with a load cell rated for 50[kN] full-scale load and Class 1 accuracy according to the ISO 7500-1 standard. The test objects have been anchored to the machine's base with custom supports while the gripper is anchored to the moving traverse, also with custom supports; Fig. 16 shows the experimental set-up. The locking/unlocking tests have been carried out by imposing a predefined motion of the moving traverse at a constant speed of 30mm/s while measuring the force values of the load cell. The displacement profile is represented in Fig. 17 (upper graph). The force exerted on the gripper has been measured and recorded during each motion cycle. The pull-out tests have been conducted with a *PCE-DFG N 500* dynamometer by PCE Instruments with a full-scale load of 500[N] and a resolution of 0.1[N]. The pieces used to test the gripper are square section parallelepipeds with a height of 60[mm] and a side length ranging from 21[mm] to 39[mm] with increments of 3[mm].

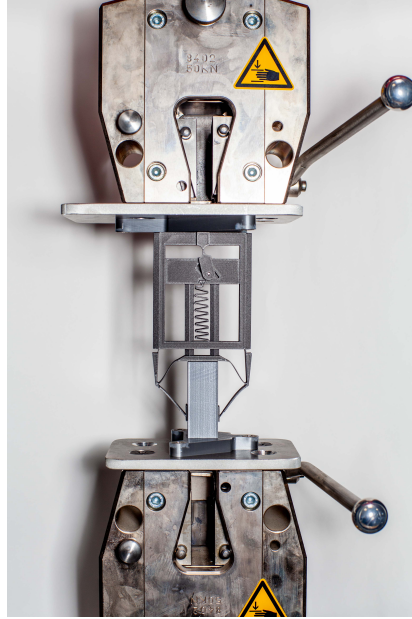


Fig. 16: Experimental set-up. The photograph represents the test set-up for the locking/unlocking tests.

### B. Results

Figure 17 shows the locking/unlocking test results without an object to be grasped. The force plot shows two peaks; the first peak corresponds to the condition required for the stable closing of the fingers, whereas the second peak corresponds to the condition where the mechanism unlocks and the fingers open. In the condition where the mechanism is locked, the load recorded by the machine's load cell drops to values close to zero. This behavior is consistent with the design intent since once this position is reached, no load is needed to maintain it. This point presents an advantage of the current design over electrically operated grippers, as the PLG does not need to be powered to maintain the grasp (similarly to pneumatic grippers). Finally, this test provides a baseline value for the force needed to activate the mechanism, approximately 45[N]. The experiment data is also plotted in Fig. 18, clearly showing the opening and closing force-displacement cycles.

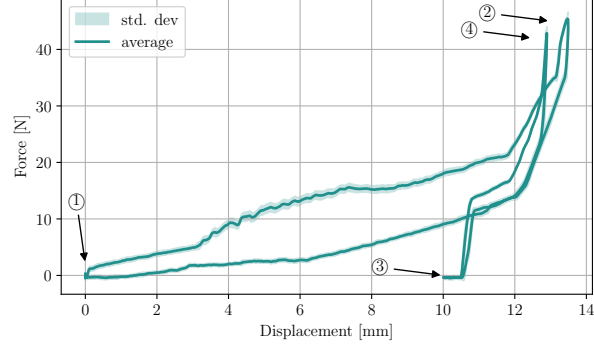


Fig. 18: Loading test without a workpiece. The graph shows the average force-displacement profile and its standard deviation.

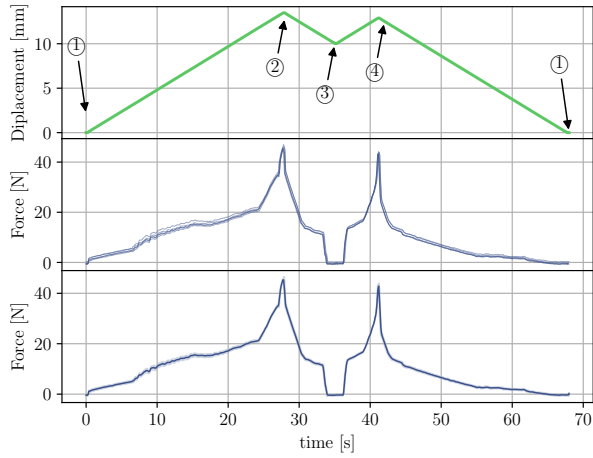


Fig. 17: Loading test without a workpiece. The top graph shows the displacement commanded to the moving traverse as a function of time. The middle graph represents the forces measured by the load cell in five test repetitions as a function of time. The bottom graph represents the average of the force profile as a function of time and its standard deviation (represented as a shaded area -barely visible).

Figure 19 presents the locking/unlocking test results with varying object sizes. The test has been repeated ten times for the seven different widths. The graph shows, as expected, the same two-peak behavior of the test without a workpiece, with force dropping to zero in the rest condition (i.e. position ③). The same picture also shows that the force needed to operate the gripper increases with the object size, from 76[N] to 83[N] for the first peak and from 76[N] to 96[N] for the second peak; this is consistent as the increase in size increases the deformation that the fingers must undergo, thus the force that must be applied to deform them. Figure 20 presents the results of the pull-out tests for the force and form closure operation modalities. The tests have been repeated ten times for each condition; the measured values have been averaged and plotted. The graph shows how the form closure operation modality allows grasping objects approximately eight times heavier than in force closure mode. Secondly, in both cases, as the object sizes increase, so do the forces needed to pull the object out of the gripper. Such force increase happens because the forces needed to deform the fingers increase as the object size increases. Hence, larger objects signify: *i*) increased contact forces, in force closure mode; *ii*) increased forces needed to deform the fingers until the grasped object would be released. In addition, Fig. 21 presents an assessment of the fidelity of the simulations by comparing the measured and simulated force profiles. The upper plot represents the force profile when activating the mechanism without an object (free condition) whereas the lower plot represents the condition when grasping an object that is 21[mm] wide. In these simulations, a friction coefficient,  $\mu = 0.3$  (found via a trial and error procedure to replicate experimental tests) has been included. A certain mismatch of the force values can be appreciated, especially in the free mechanism activation condition. This may be attributed to several factors, among which one can cite the PRB simplifications that have been introduced and the AM material (i.e. *Onyx*) may be subjected to a slight Young modulus variation after loading/unloading. Despite these differences, the salient features and the overall mechanism behavior are nicely captured by the PRB model, which also predicts the values of the peak forces with good accuracy, proving to be a useful design tool to assess the gripper behavior before

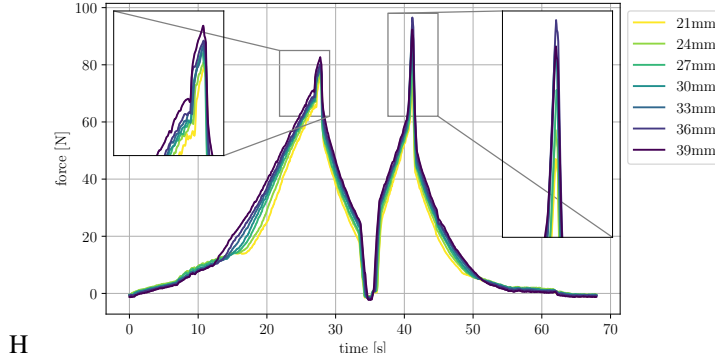


Fig. 19: Loading tests with varying workpiece sizes. The figure presents the force profiles during the grasping test with different object sizes. The test was repeated ten times for each of the seven tested object widths. The graph's curves are the average for the seven test conditions.

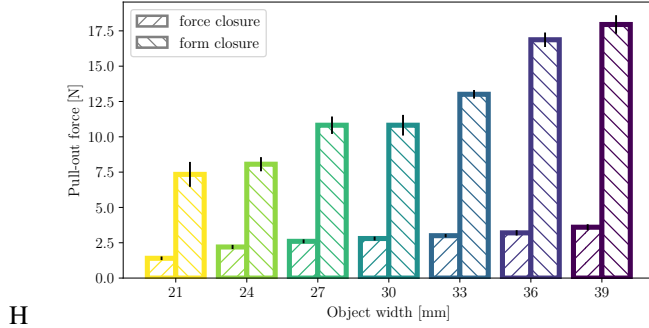


Fig. 20: Pull-out test. The figure compares the values of the forces measured in the pull-out tests for the force closure and form closure operating modalities. The test has been repeated ten times for each of the seven object sizes. The bar  $y$  values represent the average pull-out force for every object's width. The standard deviation of measurements is also represented by superimposing black error bars to every test condition.

physical prototyping. Finally, in order to provide a comparison of the presented design with state-of-the-art industrial grippers, the PLG C-factor (unit measure being [J/Kg]) has been computed and reported in Fig. 22. As defined in [2], the C-factor of a gripper can be computed as the ratio of the force it produces over its weight and multiply this ratio by the stroke. As one can see from the given plot, the presented PLG (due to its low weight and absence of actuators) outperforms most of the existing commercial solutions. In addition, the proposed solution can be manufactured at ultra-low cost, making it interesting in industrial applications where plug-and-produce, easily replaceable devices are desirable.

## V. CONCLUSIONS AND FUTURE WORK

The experiments presented in this work show how the FFF of Onyx components is a viable approach to creating a monolithic robotic gripper for pick and place operations, but also provide indications for possible improvements. At first, note that the tests carried out in this work have been limited to a few dozen of cycles. The obtained results suggest the need for further characterization of the fatigue behavior of the PLG, given the repetitive nature of the gripping operation of industrial grippers and the fact that their life often exceeds  $10^6$  cycles. Nonetheless, to date, the literature concerning the fatigue behavior of additively manufactured thermoplastics is rather scarce and additional work is necessary. A second aspect that shows potential for improvement is the ratio between the required activation force and the resulting grasping force. Even in the most favorable form closure operation modality, the value of this ratio is around 5.4, which means that to lift an object of a given weight, the gripper shall press on it with force 5.4 times this value, meaning that the push-latch design is not ideal for manipulating fragile objects. Despite the limitations mentioned above, this novel work shows how the FFF of Onyx components is already a very promising approach for creating monolithic robotic grippers for pick and place operations. Also, the experimental characterization of the end-effector demonstrates good repeatability thanks to the adoption of compliant joints. Furthermore, the simulation approach based on the PRB approximation provides a powerful, accurate and fast tool for optimizing the design and adapting it to objects and shapes of different dimensions.

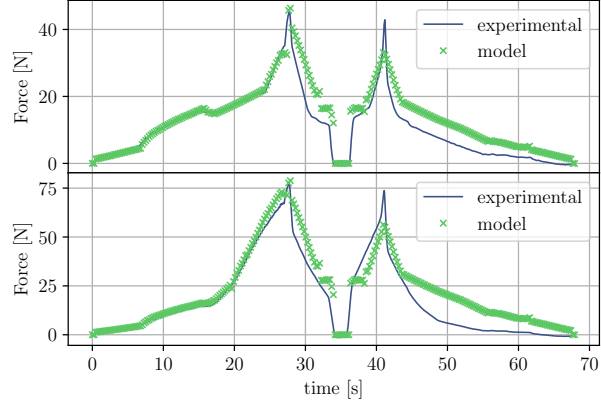


Fig. 21: Force profile comparison. The figure compares the force profile measured experimentally and the force profile derived from the model for the push-latch mechanism activation. The upper plot represents the force profile for the free condition (i.e. no object present), while the lower plot represents the force profile for the condition where an object of 21 mm width is grasped.

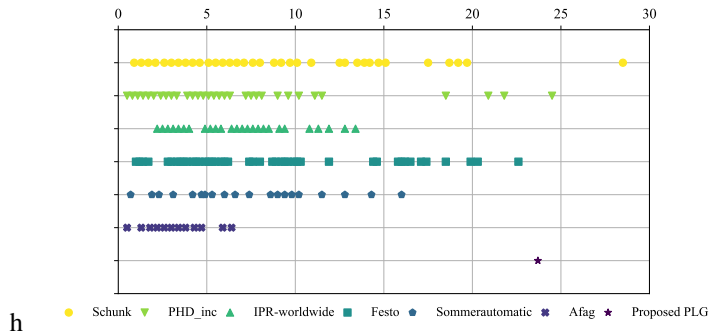


Fig. 22: Comparison of C-Factor values commonly used in the industry to those proposed in this work, adapted from [2].

## VI. ACKNOWLEDGEMENTS

We thank the staff of the IIT MWS facility (especially Lorenzo Orciari, Roberto Puddu, Marco Pinaffo and Angela Morelli) for their support in the construction of the prototypes. We thank the anonymous reviewers whose suggestions helped significantly improve the manuscript. Partially Supported by INTELLIMAN (G.A.No. 101070136), Horizon Europe, Research and Innovation Programme.

## REFERENCES

- [1] B. Zhang, Y. Xie, J. Zhou, K. Wang, and Z. Zhang, "State-of-the-art robotic grippers, grasping and control strategies, as well as their applications in agricultural robots: A review," *Computers and Electronics in Agriculture*, vol. 177, p. 105694, 2020.
- [2] L. Birglen and T. Schlicht, "A statistical review of industrial robotic grippers," *Robotics and Computer-Integrated Manufacturing*, vol. 49, pp. 88–97, 2018.
- [3] A. Petterson, T. Ohlsson, D. Caldwell, S. Davis, J. Gray, and T. Dodd, "A bernoulli principle gripper for handling of planar and 3D (food) products," *Industrial Robot: An International Journal*, vol. 37, pp. 518–526, 2010.
- [4] G. Muscato, M. Prestifilippo, N. Abbate, and I. Rizzuto, "A prototype of an orange picking robot: Past history, the new robot and experimental results," *Industrial Robot: An International Journal*, vol. 32, pp. 128–138, 2005.
- [5] R. Deimel and O. Brock, "A compliant hand based on a novel pneumatic actuator," in *2013 IEEE International Conference on Robotics and Automation*, 2013, pp. 2047–2053.
- [6] D. Drotman, S. Jadhav, M. Karimi, P. de Zonia, and M. T. Tolley, "3D printed soft actuators for a legged robot capable of navigating unstructured terrain," in *2017 IEEE International Conference on Robotics and Automation (ICRA)*, 2017, pp. 5532–5538.
- [7] L. Ge, L. Dong, D. Wang, Q. Ge, and G. Gu, "A digital light processing 3D printer for fast and high-precision fabrication of soft pneumatic actuators," *Sensors and Actuators A: Physical*, vol. 273, pp. 285–292, 2018.
- [8] R. Ma and A. Dollar, "Yale openhand project: Optimizing open-source hand designs for ease of fabrication and adoption," *IEEE Robotics & Automation Magazine*, vol. 24, no. 1, pp. 32–40, 2017.
- [9] R. Ma, J. Belter, and A. Dollar, "Hybrid deposition manufacturing: Design strategies for multimaterial mechanisms via three-dimensional printing and material deposition," *Journal of Mechanisms and Robotics*, vol. 7, p. 021002, 2015.
- [10] E. Brown, N. Rodenberg, J. Amend, A. Mozeika, E. Steltz, M. R. Zakin, H. Lipson, and H. M. Jaeger, "Universal robotic gripper based on the jamming of granular material," *Proceedings of the National Academy of Sciences*, vol. 107, no. 44, pp. 18 809–18 814, 2010.

- [11] B. Chen, Z. Shao, Z. Xie, J. Liu, F. Pan, L. He, L. Zhang, Y. Zhang, X. Ling, F. Peng, W. Yun, and L. Wen, "Soft origami gripper with variable effective length," *Advanced Intelligent Systems*, vol. 3, no. 10, p. 2000251, 2021.
- [12] Y. Tsugami and T. Nishida, "Simple structured gripper using electromagnet and permanent magnet," in *Simple Structured Gripper Using Electromagnet and Permanent Magnet*, 2017.
- [13] R. Wang, X. Zhang, B. Zhu, Z. Hongchuan, B. Chen, and H. Wang, "Topology optimization of a cable-driven soft robotic gripper," *Structural and Multidisciplinary Optimization*, vol. 62, 2020.
- [14] P. McGowan and G. Hao, "Design of a morphing compliant mechanism with separate gripping and retraction modes using a single actuation," *Journal of Mechanisms and Robotics*, vol. 15, 2022.
- [15] M. Kodnongbua, I. Good, Y. Lou, J. Lipton, and A. Schulz, "Computational design of passive grippers," *ACM Trans. Graph.*, vol. 41, no. 4, 2022.
- [16] H. Hsiao, J. Sun, H. Zhang, and J. Zhao, "A mechanically intelligent and passive gripper for aerial perching and grasping," *IEEE/ASME Transactions on Mechatronics*, vol. 27, no. 6, pp. 5243–5253, 2022.
- [17] T. Nishimura, "Push latch device," U.S. Patent 4,792,165, 1988.
- [18] M. S. Louis, "Push-push latch," U.S. Patent US 6,669,250 B1, 2003.
- [19] T. S. King and K. R. Levey, "Push/push latch," U.S. Patent US 7,793,995 B2, 2010.
- [20] X. Su, Y. Yang, D. Xiao, and y. Chen, "Processability investigation of non-assembly mechanisms for powder bed fusion process," *The International Journal of Advanced Manufacturing Technology*, vol. 64, 2012.
- [21] "Automation technology and technical education solutions | Festo GB," Visited on: 2023-01-10. [Online]. Available: <https://www.festo.com/>
- [22] "Schunk," Visited on: 2023-01-10. [Online]. Available: <https://schunk.com/>
- [23] "BTM Europe - State of the Art Clinching Systems," Visited on: 2023-01-10. [Online]. Available: <https://www.btm-europe.de/>
- [24] K. Lussenburg, A. Sakes, and P. Breedveld, "Design of non-assembly mechanisms: A state-of-the-art review," *Additive Manufacturing*, vol. 39, p. 101846, 2021.
- [25] L. Kiener, H. Saudan, F. Cosandier, G. Perruchoud, and P. Spanoudakis, "Innovative concept of compliant mechanisms made by additive manufacturing," *MATEC Web of Conferences*, vol. 304, p. 07002, 2019.
- [26] R. M. Fowler, A. Maselli, P. Pluimers, S. P. Magleby, and L. L. Howell, "Flex-16: A large-displacement monolithic compliant rotational hinge," *Mechanism and Machine Theory*, vol. 82, pp. 203–217, 2014.
- [27] A. Bruyas, F. Geiskopf, and P. Renaud, "Design and modeling of a large amplitude compliant revolute joint: The helical shape compliant joint," *Journal of Mechanical Design*, vol. 137, p. 085003, 2015.
- [28] L. L. Howell, S. P. Magleby, and B. M. Olsen, *Handbook of Compliant Mechanisms*. Wiley, 2013, cited by: 433.
- [29] F. Calignano, D. Manfredi, E. P. Ambrosio, S. Biamino, M. Lombardi, E. Atzeni, A. Salmi, P. Minetola, L. Iuliano, and P. Fino, "Overview on additive manufacturing technologies," *Proceedings of the IEEE*, vol. 105, no. 4, pp. 593–612, 2017.
- [30] P. Bilancia, G. Berselli, L. Bruzzone, and P. Fanghella, "A CAD/CAE integration framework for analyzing and designing spatial compliant mechanisms via pseudo-rigid-body methods," *Robotics and Computer-Integrated Manufacturing*, vol. 56, pp. 287–302, 2019.
- [31] F. Bárnik, M. Vaško, M. Handrik, F. Dorčíak, and J. Majko, "Comparing mechanical properties of composites structures on onyx base with different density and shape of fill," *Transportation Research Procedia*, vol. 40, pp. 616–622, 2019, tRANSCom 2019 13th International Scientific Conference on Sustainable, Modern and Safe Transport.
- [32] H. R. Vanaei, A. E. Magri, M. A. Rastak, S. Vanaei, S. Vaudreuil, and A. Tcharkhtchi, "Numerical - experimental analysis toward the strain rate sensitivity of 3D-printed nylon reinforced by short carbon fiber," *Materials*, vol. 15, no. 24, 2022.
- [33] P. Bilancia, G. Berselli, L. Bruzzone, and P. Fanghella, "A Practical Method for Determining the Pseudo-rigid-body Parameters of Spatial Compliant Mechanisms via CAE Tools," *Procedia Manufacturing*, vol. 11, pp. 1709–1717, 2017.
- [34] V. K. Venkiteswaran and H.-J. Su, "A parameter optimization framework for determining the pseudo-rigid-body model of cantilever-beams," *Precision Engineering*, vol. 40, pp. 46–54, 2015.